



HAL
open science

Upper Pleistocene uplifted shorelines as tracers of (local rather than global) subduction dynamics

H. Henry, V. Regard, Kevin Pedroja, L. Husson, J. Martinod, C. Witt,
Arnauld Heuret

► To cite this version:

H. Henry, V. Regard, Kevin Pedroja, L. Husson, J. Martinod, et al.. Upper Pleistocene uplifted shorelines as tracers of (local rather than global) subduction dynamics. *Journal of Geodynamics*, 2014, 78, pp.8-20. 10.1016/j.jog.2014.04.001 . hal-00968538

HAL Id: hal-00968538

<https://hal.science/hal-00968538>

Submitted on 1 Apr 2014

HAL is a multi-disciplinary open access archive for the deposit and dissemination of scientific research documents, whether they are published or not. The documents may come from teaching and research institutions in France or abroad, or from public or private research centers.

L'archive ouverte pluridisciplinaire **HAL**, est destinée au dépôt et à la diffusion de documents scientifiques de niveau recherche, publiés ou non, émanant des établissements d'enseignement et de recherche français ou étrangers, des laboratoires publics ou privés.

1
2 **UPPER PLEISTOCENE UPLIFTED SHORELINES AS TRACERS OF (LOCAL RATHER THAN**
3 **GLOBAL) SUBDUCTION DYNAMICS**
4

5
6 Hadrien Henry^{1,2,3}, Vincent Regard^{1,2,3*}, Kevin Pedoja^{4,5,6}, Laurent Husson⁷, Joseph
7 Martinod^{1,2,3}, Cesar Witt⁸, Arnauld Heuret⁹
8

9 1- Université de Toulouse; UPS GET, 14 avenue E. Belin, F-31400 Toulouse, France

10 2- CNRS; GET ; 14 avenue E. Belin, F-31400, Toulouse, France

11 3- IRD; UR 234, GET ; 14 avenue E. Belin, F-31400, Toulouse, France

12 4- Normandie Univ, France

13 5- UCBN, M2C, F-14000 Caen, France

14 6- CNRS, UMR 6143 M2C, F-14000 Caen, France

15 7- CNRS, ISTERRE, Université Joseph Fourier, Grenoble, France

16 8- Université de Lille 1; CNRS ; Géosystèmes, Villeneuve D'Ascq, France

17 9- Département de Géologie; EA4098 LaRGe Labo. de Rech. en Géosciences; Université des
18 Antilles et de la Guyane, Campus de Fouillol - 97159 Pointe à Pitre Cedex, Guadeloupe,
19 FWI.

20 * Corresponding author. E.mail: Vincent.regard@get.obs-mip.fr; Ph : +33 5 61332645
21

22 **ABSTRACT**
23

24 Past studies have shown that high coastal uplift rates are restricted to active areas, especially
25 in a subduction context. The origin of coastal uplift in subduction zones, however, has not yet
26 been globally investigated. Quaternary shorelines correlated to the last interglacial maximum
27 (MIS 5e) were defined as a global tectonic benchmark (Pedoja et al. (2011)). In order to
28 investigate the relationships between the vertical motion and the subduction dynamic
29 parameters, we cross-linked this coastal uplift database with the "geodynamical" databases
30 from Heuret (2005), Conrad and Husson (2009) and Müller et al. (2008). Our statistical study
31 shows that: [1] the most intuitive parameters one can think responsible for coastal uplift (e.g.,
32 subduction obliquity, trench motion, oceanic crust age, interplate friction and force,
33 convergence variation, dynamic topography, overriding and subducted plate velocity) are not
34 related with the uplift (and its magnitude); [2] the only intuitive parameter is the distance to
35 the trench which shows in specific areas a decrease from the trench up to a distance of ~300
36 km; [3] the slab dip (especially the deep slab dip), the position along the trench and the
37 overriding plate tectonic regime are correlated with the coastal uplift, probably reflecting
38 transient changes in subduction parameters. Finally we conclude that the first order parameter
39 explaining coastal uplift is small-scale heterogeneities of the subducting plate, as for instance
40 subducting aseismic ridges. The influence of large-scale geodynamic setting of subduction
41 zones is secondary.
42
43

44 **Highlights**
45

- 46 - Large-scale geodynamics only explain first order coastal uplift rates
47 - Uplift is localized over asperities of the subducting plate
48 - Uplift could be related to transient changes in subduction parameters

49 - Rapid uplift is restricted to the area <300 km from the trench (forearc)

50 - Forearc and plate interiors respond differently

51

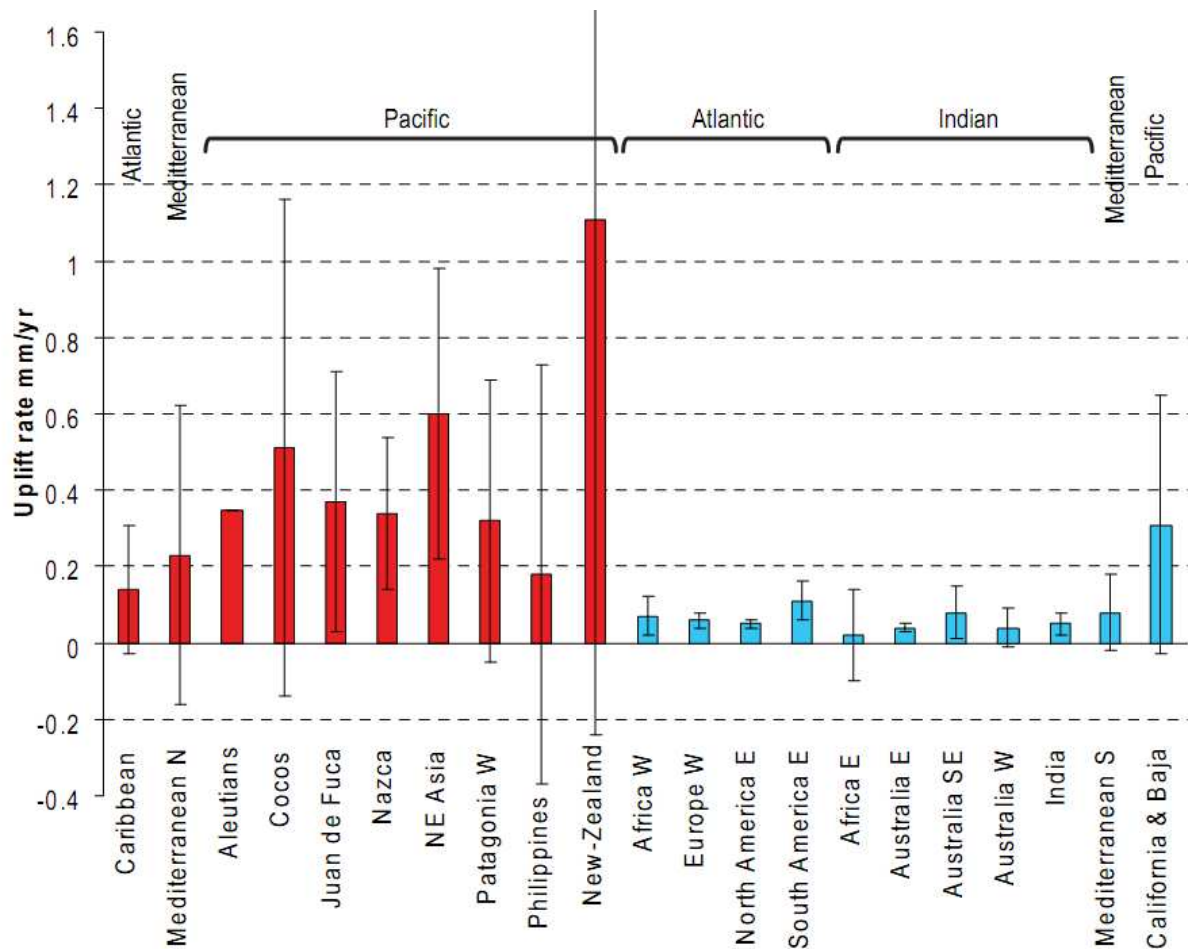
52 **Keywords:** marine strandline; shoreline; uplift; subduction; geodynamics; Quaternary

53 1. INTRODUCTION

54

55 Fossil shorelines (or strandlines) are generally packed and constitute staircase coastal
56 geomorphologies or sequences of "terraces" (e.g. marine or reefal for example). They are
57 tracers of the sea level at the time they formed. Current elevation of fossil shorelines results
58 from the combination of sea level change (eustasy) and vertical ground motion (uplift or
59 subsidence, Lajoie et al. (1991), Pirazzoli et al. (1993)). Pedoja et al. (2011) exhaustively
60 compiled the worldwide repartition and elevation of the shorelines formed during the last
61 interglacial sea level highstand (Marine Isotopic Stage 5e, ~120 ka BP) and calculated
62 apparent coastal uplift rates since that time. More recently, Pedoja et al. (in press),
63 investigated other benchmarks (MIS 1, 3, 11 and upper shoreline of the sequences) in the
64 coastal sequences including MIS 5e strandline. Their database highlights the contrast in
65 tectonic uplift rates between active zones (mainly Pacific Ocean) and passive zones (Atlantic
66 and Indian Oceans) (Figure1). Even if Pedoja et al. (in press) did a first-order exploration of
67 uplift record on paleoshorelines in function of the rough geodynamic setting, vertical motion
68 along the coasts located above subduction zones has never been extensively explored. In this
69 paper, we look for possible geological parameters that may explain why coastal areas located
70 above subduction zones are uplifting so fast (Figure 1).

71



72
73 *Figure 1. Worldwide distribution of apparent coastal uplift rates (since MIS 5e): in red and blue the*
74 *average uplift rate for, respectively, the actively deforming zones (mostly subduction zones) and the*
75 *stable zones (mostly passive margins; data from Pedoja et al. (2011)). Brackets represent the data*
76 *standard deviation. Note the zone named California and Baja, corresponds to a passive margin very*
77 *close to a rift/transform setting.*

78 The compilation from Pedoja et al. (2011) records only emerged terraces with few exceptions.
79 As discussed in Pedoja et al. (2011), the worldwide distribution of shoreline sequences
80 suggests that there are much less subsiding areas along subduction coastlines than uplifting
81 ones, a fact that shall not be considered as an observational bias (see Pedoja et al., 2011,
82 2014). Then, the database may reflect a global tendency to coastal uplift during late
83 Pleistocene (Pedoja et al. (2011)), and also partly results from the fact that Pleistocene to
84 present-day coastal subsidence is more difficult to quantify than coastal uplift. In any case,
85 this database shows that the average coastal uplift is faster above subduction zones than at
86 passive margins. In the following, we look for possible links between Late Pleistocene
87 (posterior to MIS5) coastal uplift and subduction geodynamics. In particular, we investigate
88 the uplift dependence on some geodynamic parameters, chosen for their driving effect. Some
89 are obvious, like: distance to the trench, trench motion, age of the subducting plate,
90 subduction obliquity, overriding and subducting plate velocities, and dynamic topography.
91 The others are suspected to act on the vertical motion but with magnitudes and direction that
92 deserve exploration: interplate force and friction force, position along the trench (i.e. distance
93 to the subducting plate edge), slab dip, tectonic setting of the overriding plate (see Heuret,
94 2005).

96 **2.1 Databases: paleoshorelines and geodynamics**

97 The compilation by Pedoja et al. (in press); Pedoja et al. (2011) focuses on coastal
98 geomorphic indicators correlated to the Marine Isotopic Stage 5e (125 ky BP). Indeed,
99 corresponding terraces are the most extensively preserved and dated. Moreover, MIS 5e is
100 purportedly the last analogue to the current interglacial and the time span is enough to largely
101 exceed several seismic cycles such that the uplift rate is not significantly affected by an
102 individual seismic event. Using the MIS 5e shoreline elevation, we calculated the average
103 uplift rate using the following formula: $U=(z-e)/t$, with U the shoreline uplift rate, z the MIS
104 5e terrace elevation, t the age of the terrace and e the relative elevation of the MIS 5e sea level
105 with respect to the current sea level. In accordance to Pedoja et al. (in press); Pedoja et al.
106 (2011)), we use $e= 0\pm 10$ m, which is conservative in the sense it takes into account the
107 different debated evaluations of the last interglacial sea-level (e.g., Waelbroeck et al. (2002),
108 Kopp et al. (2009); O'Leary et al. (2013)) and the way the shorelines are fossilized (e.g.,
109 Lajoie et al. (1991)). In addition, this elevation value is of little interest to the current study as
110 it uniformly offsets uplift rates while our analysis considers relative vertical displacements
111 from one site to another. Besides the elevation of the uplifted shorelines, Pedoja et al. (in
112 press; 2011) deliver some additional information like the geographic location of the
113 sequences. Noteworthy, the spatial repartition of the data over South America, Japan and
114 Cascadia subduction allow investigating the coastal uplift distribution as a function of the
115 distance to the trench up to 800 km away (in the Japan and South America transects). In
116 addition, it is noticeable that some places have not been investigated for marine terraces, like
117 the Aleutian subduction zone where the Ostrov Beringa and Seguam islands exhibit marine
118 terraces visible on satellite images but not studied in the field or even the Mariana subduction
119 zone (Stafford et al. (2005) observed uplifted karst in Guam).

120
121 Subduction zone geodynamic parameters are sourced from Heuret (2005)(parts of the data
122 base have been published in Heuret & Lallemand, 2005, Lallemand et al., 2005 and Funiciello
123 et al. 2008). He provides every 2 degrees multiple geodynamic parameters like the overriding
124 plates tectonic regime, the trench motion, the proximity of the measurement to a subduction
125 edge, the shallow and deep slab dip, the age of the adjacent oceanic crust and the plate
126 convergence rate. In addition, we extracted the current dynamic topography rate of change for
127 the last Myr from the dynamic topography data released by Conrad and Husson (2009) and
128 Müller et al. (2008). Besides end-member models HS3 (Gripp and Gordon 2002) or NNR ,
129 most of the reference frames fall in the same range (see e.g. fig.6 in Becker, 2006). Given
130 that, we chose the moving hotspot model of Steinberger et al. (2004) to calculate the trench,
131 the overriding and subducting absolute plate motion because we see it as representative of
132 most frameworks (see Funiciello et al for some comparisons between frameworks). Thus, we
133 emphasize that our observations and conclusions would not be altered by choosing an
134 alternative reference frame. The reference frame defined by Steinberger et al. (2004) is very
135 similar to that of O'Neill et al. (2005) which is based on the Indo-Atlantic hotspots. Such
136 reference frames are most in line with predictions from geodynamic models where subducting
137 plates move trenchward and trenches predominantly retreat and where global mantle viscous
138 dissipation is minimized, while this is not the case for HS3 (Schellart et al., 2008). Second,
139 Indo-Atlantic hotspots reference frames are in better agreement with observed global mantle
140 anisotropy than HS3 (Becker et al., 2008, Kreemer, 2009) and with subducted slab structure
141 than HS3 (Schellart, GRL 2011). The convergence rates are extracted from Heuret (2005)
142 (published in Lallemand et al., 2005).

143 The interplate friction force is calculated after Lallemand (1999) assuming a friction
144 coefficient of 0.3. The interplate force at trench is probably best expressed as the mean trench
145 normal integrated mantle drag called M_d and calculated by Husson (2012). This metric
146 averages the drag forces exerted by the convecting mantle underneath the converging plates.
147 This value is the integral of the normal to trench components of the shear tractions derived
148 from Conrad and Behn (2010) or Conrad and Husson (2009). As, such
149 it is a measure of the net horizontal force that drags plates against each other. Husson (2012)
150 proposed this value to be best correlated to the upper plate tectonic setting (see thereafter,
151 section 3.3).

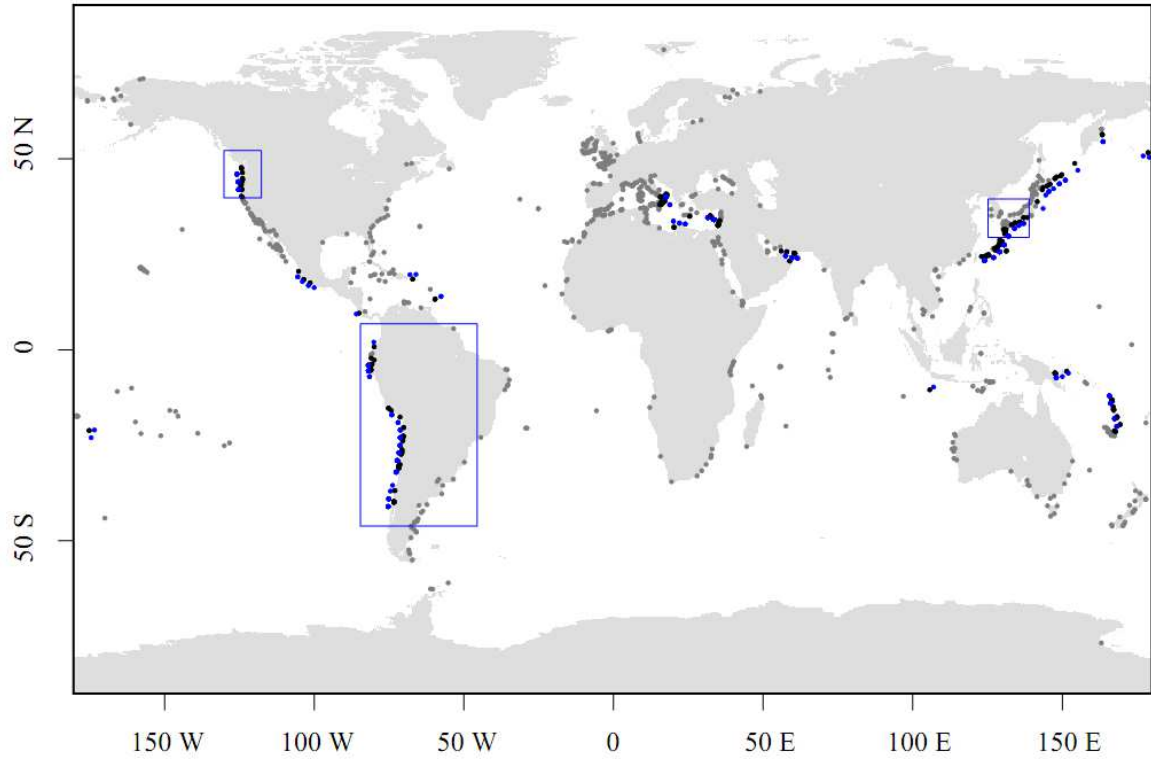
152 The Mediterranean Sea has been avoided by Heuret (2005) because subduction zones are
153 small and possibly interact with each other and surrounding collision zones. The dataset of
154 Heuret (2005) is here extended to encompass the Mediterranean Sea (Gibraltar, Tyrrhenian
155 and Aegean subduction zones) and the Makran (Figure 2A).

156
157 Finally, we combine the 2 datasets (uplifted shorelines from the last interglacial maximum vs.
158 subduction geodynamics), by associating each site of uplifted shoreline to the closest
159 subduction data point in 2 degree-bins. Figure 2 shows the spatial repartition of the uplifted
160 paleocoasts (shoreline, strandline, etc.) and related subduction record. The average uplift rate
161 derived from the marine terraces in this record is ~ 0.2227 mm/y.

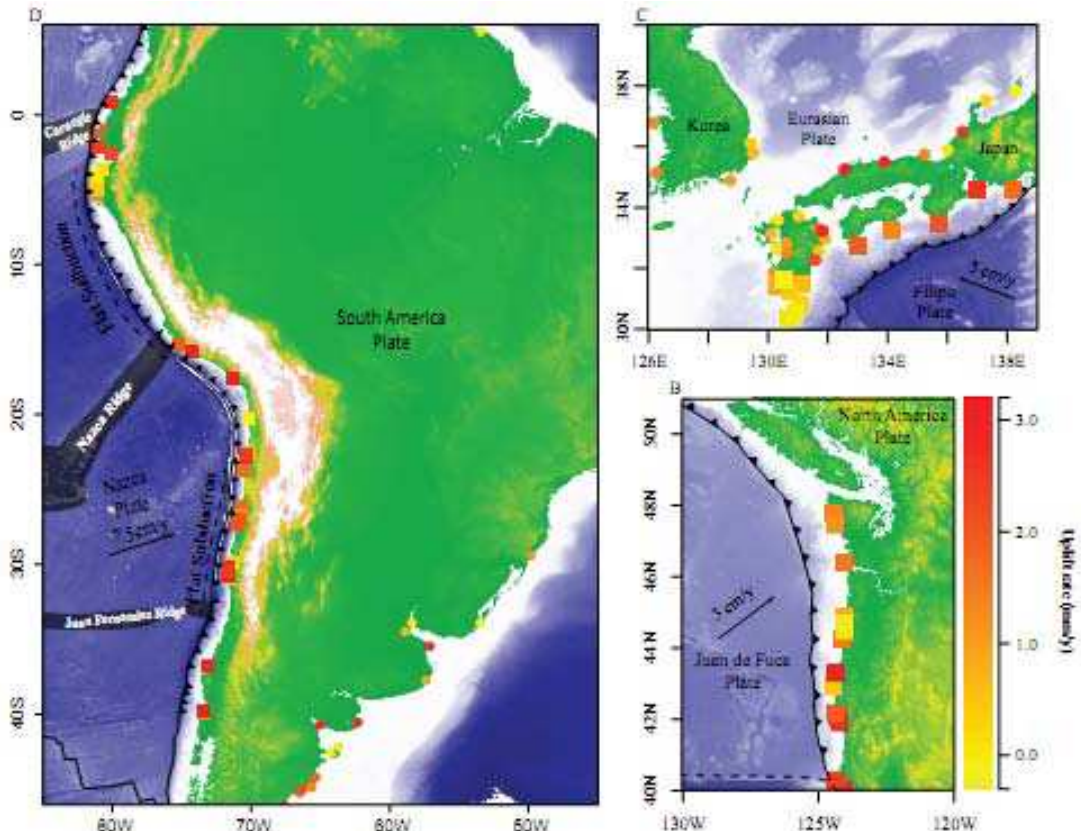
162
163 In order to define a robust indicator of correlation between the apparent coastal uplift rate and
164 the various geodynamic parameters that we tested, we calculated correlation coefficients r as
165 defined by Pearson (1896):

166
$$r = \frac{\sum_{i=1}^n (x_i - \bar{x})(y_i - \bar{y})}{\sqrt{\sum_{i=1}^n (x_i - \bar{x})^2 \sum_{i=1}^n (y_i - \bar{y})^2}}$$

167 where x_i and y_i are data coordinates and \bar{x} and \bar{y} their average values. A correlation coefficient
168 of 1 or -1 would respectively indicate a perfect linear correlation or anti-correlation between
169 the uplift rate and the tested parameter. Every data manipulation and calculation has been
170 performed with the software RGui (R Development Core Team (2010)). Note that this
171 correlation coefficient is ineffective to account for non-linear relationships. We will qualify of
172 ‘significant’ every correlation coefficient associated with a p-value < 0.01. This always comes
173 with a 1σ confidence interval encompassing the 0 value.



175 A



176
177
178
179
180
181

Figure 2. A. Spatial repartition of the two main databases: the MIS 5e uplifted shoreline data from Pedoja et al. (2011) are in grey or black if less than 2 degrees away from any subduction data (Heuret and Lallemand, 2005) ; the subduction data, in blue is only pictured if MIS5e uplifted shoreline data are associated. The blue boxes display the three places where records are suitable to observe the uplift rate distribution along a trench perpendicular transect. B to D, zoom on areas of

182 *special interest (see transects, sections 2.2 and 3.1); colours represent the uplift rate and the symbol*
183 *(square/circle) represent the location of data less/more than 2degrees away from the trench.*

184 **2.2 Geological context of the South America, Cascadia and Japan-Korea** 185 **margins**

186 We found 3 places in the world where a repartition of terrace data from the fore-arc area
187 toward the inner upper plate is available (Figure 2): the Juan de Fuca plate subduction under
188 the Cascades, the Nazca plate subduction under South America and the Philippine Sea plate
189 subduction under Japan and Korea. The Juan de Fuca plate subduction zone extends
190 ~1000 km from the north of the Mendocino triple point to the south of the Queen Charlotte
191 Island (51°N/130°W; 40°N/110°W). The subduction obliquity varies from 30° to the south to
192 15° to the north with a plate convergence rate estimated at 3.1 cm/y (Heuret and Lallemand,
193 2005). The age of the oceanic crust entering the trench is 10 My (Müller et al. (1997)). The
194 tectonic setting of the overriding plate varies from slightly extensive to the south to mostly
195 wrench faulting to the north (E1 to 0 as described thereafter; Heuret and Lallemand, 2005).
196 The distance between the location of uplift data and the trench varies between 60 and 135 km
197 (Figure 3B). The upper plate lithosphere elastic thickness is 10-30 km (Lowry et al. (2000)).

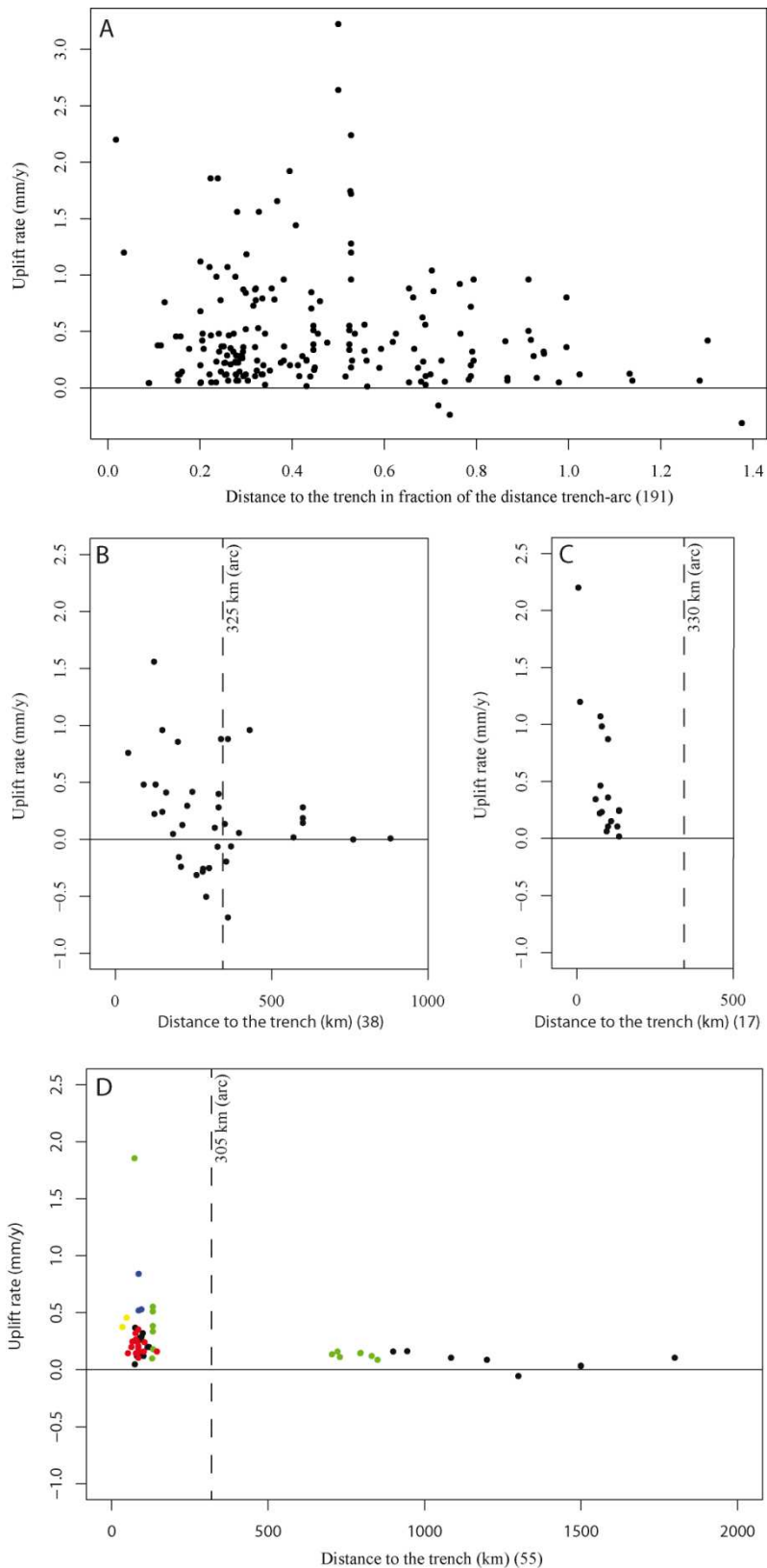
198 Coastal sequences on the Japan/Korea coasts are located above the Nankai-Ryukyu
199 subduction zone where the Philippine Sea plate subducts below the Eurasian plate. This area
200 extends latitudinally from Tokyo to Pyongyang, and from Honshu Island to the Tanega-Shima
201 Island from E to W (40°N/126°E; 30°N/139°E). The obliquity of the subduction ranges from
202 20° to the west to 40° to the east (Heuret and Lallemand, 2005). Plate convergence in this area
203 is 4.8 cm/y and the oceanic crust entering the trench is 35 My-old (Müller et al. (1997)). The
204 tectonic setting of the Eurasian plate is slightly compressive on the whole studied segment
205 (C1 as described thereafter) (Heuret and Lallemand, 2005). In this area, the distance between
206 uplift data and the trench varies between 60 and 900 km (Figure 3A).

207 The South American area analyzed in this study is located along the ~6000 km-long Nazca
208 subduction zone (from 5°N to 45°S, figure 2D). The Nazca subduction presents several
209 particular zones of interest: the Carnegie ridge (0.5°N to 2°S; Gutscher et al. (1999a)), the
210 Peruvian flat subduction (2 to 15°S, Gutscher et al. (1999b)), the Nazca ridge entrance into
211 subduction (13 to 16°S; e.g., Machare and Ortlieb (1992), Hampel (2002), Espurt et al.
212 (2008), Saillard et al. (2011)) and the Andean flat slab region which is located between 27 and
213 32° S (Yañez et al. (2001)). Plate convergence in this area is about 7 cm/y and the oceanic
214 crust entering into the trench is 0 to 40 My-old (Müller et al. (1997); Heuret and Lallemand,
215 2005). Subduction obliquity is everywhere smaller than 20°. The South American plate
216 tectonic setting presents a North to South compression gradient (Heuret and Lallemand,
217 2005), from compressive in Central Andes to neutral in Southern Andes; its elastic thickness
218 possibly strongly varies from less than 10 km along the arc to >50 km in the foreland (Tassara
219 (2005); Tassara et al. (2007)).

220 **3. RESULTS**

221 **3.1 Distance to the trench**

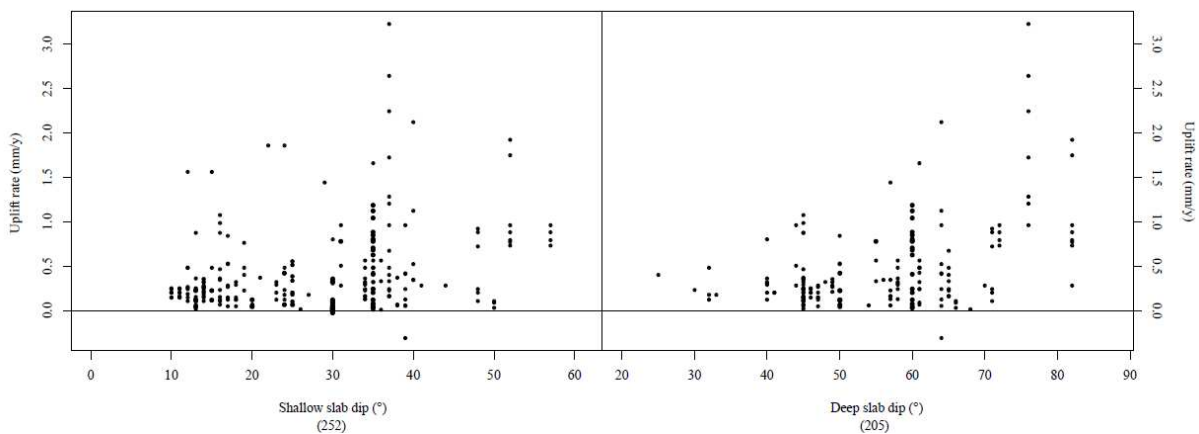
222



223
 224 *Figure 3. Uplift rate versus distance to the trench. A: All data, expressed in function of the trench-*
 225 *arc distance. B: Philippine Sea plate subduction. C: Cascadia subduction. D: Nazca subduction;*
 226 *data located above the Peruvian and the Juan Fernandez flat subduction areas are shown in red (2-*
 227 *15°S and 27-32°S), over the Nazca Ridge in blue (13-16°S) and over the Carnegie Ridge in yellow*
 228 *(0.5°N-2°S). In addition green points are data from Patagonia (south of 32°S).*

229 The distance to the trench anti-correlates with uplift rates (Figure 3). Higher uplift rates are
 230 found at the closest points to the trench in every transect (Figure 3). Uplift rates generally
 231 decrease with the distance to the trench, with sometimes an area of slower uplift (e.g.,
 232 negative values at ~300 km from the trench in Japan, Figure 3B). A direct correlation between
 233 the distance to the trench and the uplift rate is clear close to the trench, less clear farther. The
 234 overall relation is marked by a negative correlation coefficient of -0.12 (<-0.24 for each
 235 individual zone, table 3), quite significant (p-value of 0.03), which is meaningless considering
 236 the trend is non-linear (it becomes non-linear when considering points farther than the arc,
 237 Figure 3). We observe that the area of strong uplift is restricted to the first ~300 km from the
 238 trench, corresponding to the forearc area.

239 3.2 Slab dip

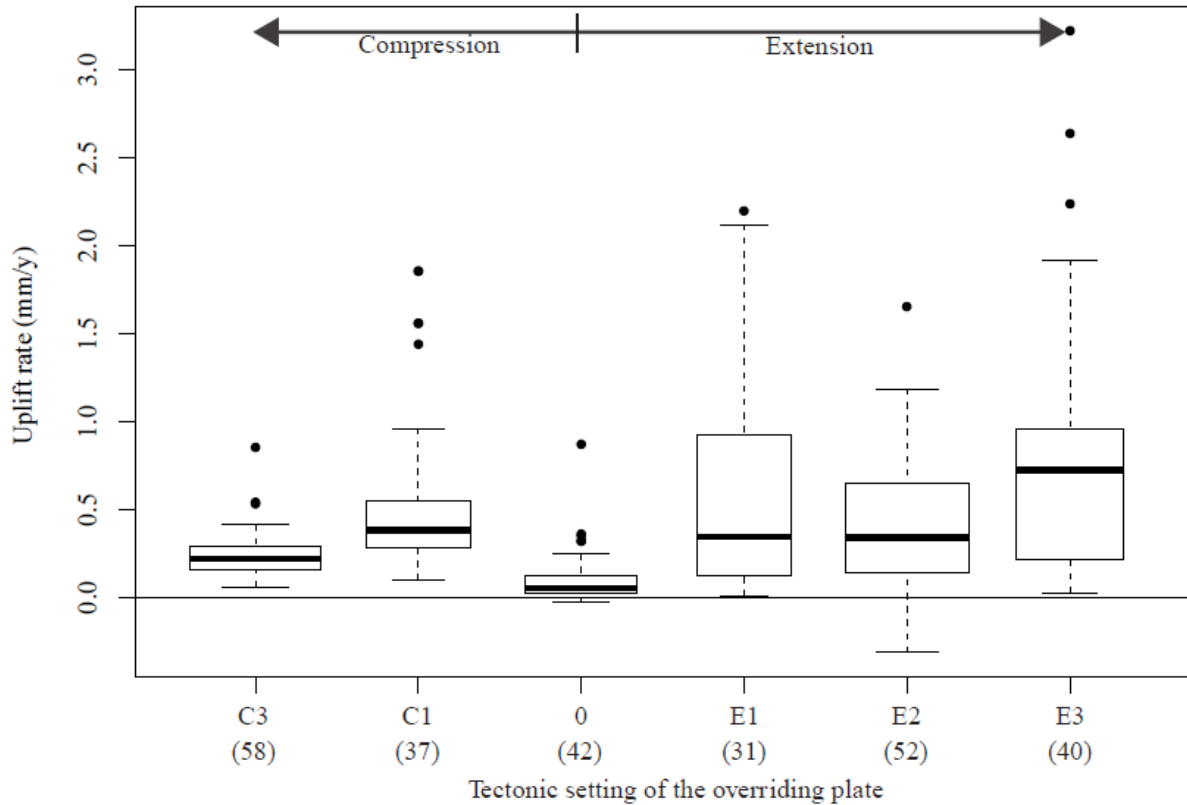


240 *Figure 4. Left: uplift rate vs. shallow slab dip; right: uplift rate vs. deep slab dip, for the entire*
 241 *dataset.*

242 Slab dip is measured at shallow depth (average dip between 0 and 125 km depth); and at
 243 greater depth, (average dip between 125 and 670 km depth)(Heuret and Lallemand, 2005).
 244 For both shallow and deep slab dip datasets, corresponding uplift rate appears to increase with
 245 slab dip (Figure 4). For the shallow slab dip the correlation is not obvious but marked by a
 246 slightly positive correlation coefficient of 0.32. The deep slab dip does not seem to influence
 247 the uplift rate below a critical value of ~60 degrees; above this value, there is a positive
 248 correlation between deep slab dip and surface uplift (Figure 4).

249 3.3 Tectonic setting of the overriding plate

250 Figure 5 shows the variations of uplift rate in function of the tectonic regime of the overriding
 251 plate. Heuret (2005) and Heuret and Lallemand (2005) describe the tectonic regime of the
 252 overriding plate using recorded focal mechanisms and classify it from the very compressive
 253 (C3) to very extensive (E3), 0 being neutral (no focal mechanism or wrench faulting). For this
 254 kind of qualitative parameter, it is not possible to calculate a correlation coefficient. We rather
 255 study them qualitatively, using boxplots (sometimes called box-and-whisker plots Tukey,
 256 1977).
 257



258
 259 *Figure 5. Uplift rate as a function of the overriding plate tectonic setting as defined by Heuret and*
 260 *Lallemand (2005). C3 is considered to be the most compressive state while E3 is the most*
 261 *extensional. C2 is absent because no C2 area is related to MIS5e marine terraces. Data number*
 262 *appears in parentheses under each box. Additional information can be found in Table 1. Horizontal*
 263 *bars indicate, from the bottom to the top, the first decile, the first quartile, the median, the third*
 264 *quartile and the ninth decile; dots are outliers. The horizontal size of the box is function of the data*
 265 *number.*

266 Figure 5 shows a slight tendency to greater uplift rates when the tectonic setting is extensional
 267 rather than compressive. Noteworthy, intermediate settings (C1 to E2) are quite similar while
 268 the main trend comes from the extremes (C3 and E3 tectonic settings).
 269

270 *Table 1. Mean uplift rates (mm/yr) as a function of the tectonic setting of the overriding plate (C3*
 271 *to E3) and for the position along the subduction zone expressed in “far” or “at” slab edge.*

	C3	C2	C1	0	E1	E2	E3	At slab edge	Far from slab edge	Accretionary margins	Erosive margins
1 st quartile	0.144	NA	0.280	0.020	0.120	0.144	0.212	0.100	0.144	0.160	0.144
Median	0.208	NA	0.384	0.054	0.344	0.340	0.724	0.328	0.240	0.364	0.244
3 rd quartile	0.280	NA	0.550	0.120	0.928	0.652	0.950	0.872	0.364	0.780	0.406
Number of	58	NA	37	42	31	52	40	113	147	112	148

data											
------	--	--	--	--	--	--	--	--	--	--	--

272
273
274
275
276
277
278
279
280
281
282

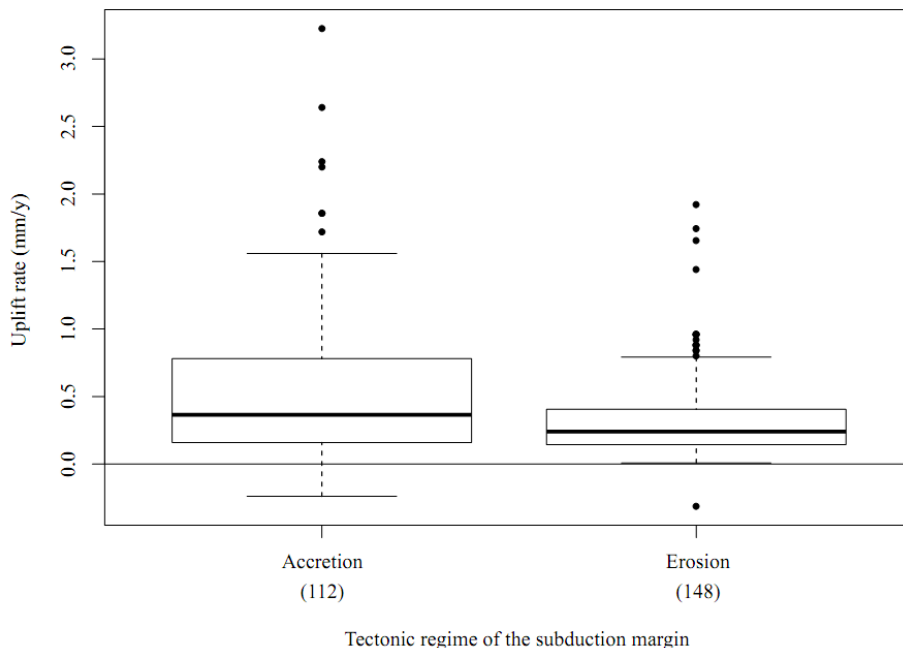
Figure 6 shows the relation between the uplift rate and the tectonic regime of the subduction margin. Accretionary margins show a higher magnitude (median: 0.36 mm/yr instead of 0.24 mm/yr for erosive ones) and a greater variability in uplift rate than erosive margins. The difference between those two regimes is somewhat significant: the median value for the accretionary margin (0.36 mm/y) corresponding to the third quartile value of the erosive margins (0.41 mm/y). The frequency of observation of uplift/subsidence in accretionary and erosive margins does not differ significantly (Table 2). This, together with the figure 6 pleads for a more variable vertical motion at accretionary margins than at erosive ones but without preferential (uplift/subsidence) direction.

283
284
285
286

Table 2. Number of data showing uplift, subsidence as function of the subduction margin tectonic setting. It reads as following example: the dataset of accretionary margins over 139 data, 26 (19%) record uplift and 2 (1%) record subsidence. There is no vertical motion data for the remaining 111 (80%) data.

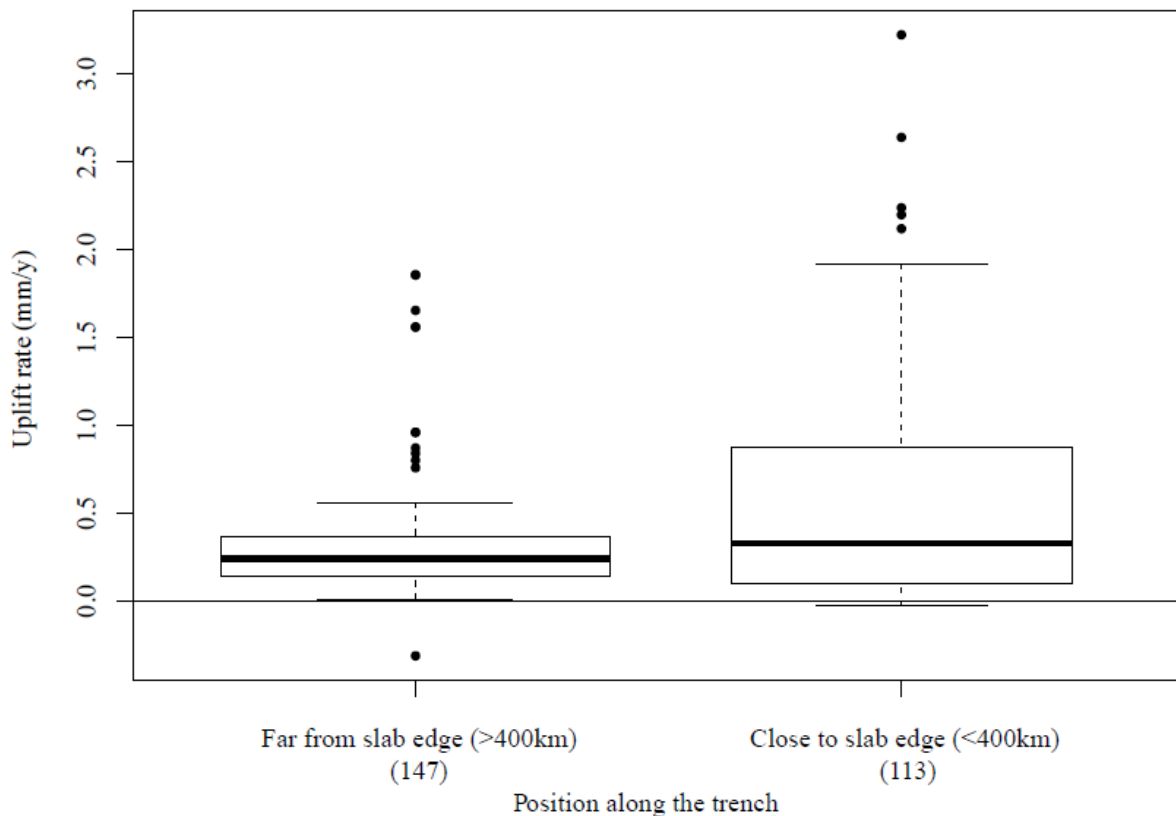
	Accretionary	%	Erosive	%
Number of data	139		121	
Uplift	26	19	40	33
Subsidence	2	1	1	1
No associated data	111	80	80	66

287



288
289
290
291

Figure 6. Uplift rate as a function of the subduction margin tectonic setting. See caption of Figure 5 for description of figure. Data number appears in parentheses under each box.



293 *Figure 7. Uplift rate versus distance to a subduction edge. See caption of Figure 5 for description of*
 294 *figure. Data number appears in parentheses under each box. Additional information can be found*
 295 *in Table 1.*
 296

297 The position along the trench may be an important parameter as emphasized by the particular
 298 tectonic setting of slab lateral boundaries (Funiciello et al. (2004); Lallemand et al. (2005);
 299 Schellart et al. (2011)). According to Lallemand et al. (2005), a datum is considered to be at a
 300 subduction edge if it is closer than four degrees from the edge of the subduction. The uplift
 301 rate is shown as a function of the proximity of the measurement to a slab edge in figure 7.
 302 This figure shows that slab edges are characterized by higher uplift rates than elsewhere along
 303 the subduction zone. The difference is somewhat significant: the median value at slab edge
 304 corresponds to the third quartile value far from the edges (average uplift rate of 0.33 and 0.36
 305 mm/y, respectively, Table 1).

306 **3.5 Dynamic topography**

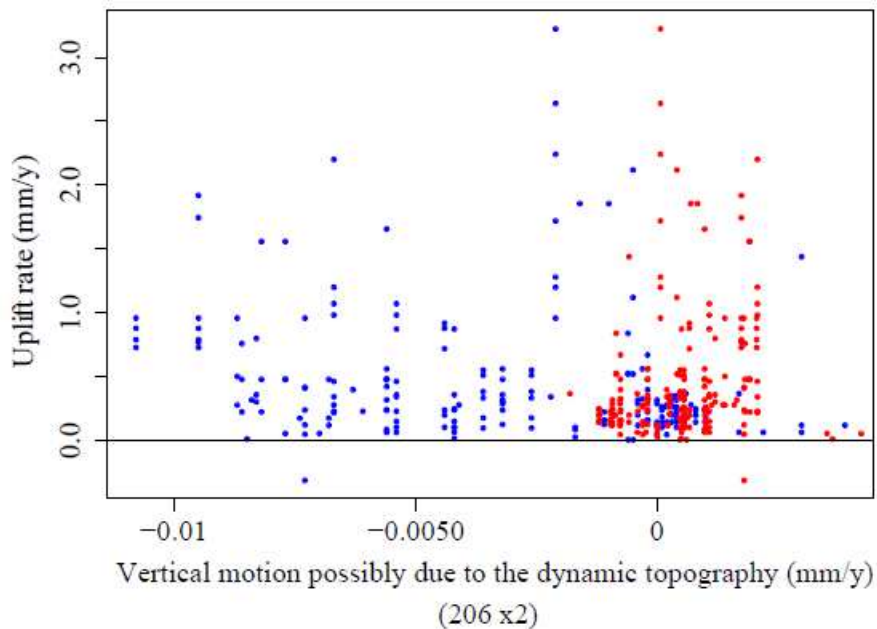
307 Temporal changes in dynamic topography can offset sea level relative to the continent. A local
 308 decrease in dynamic topography leads to sea transgression while and conversely, an increase
 309 will produce continent emersion, regression, marine terrace fossilization and uplift. Thus we
 310 calculated the rate of change in dynamic topography through the last million years. Two
 311 models of dynamic topography change have been tested (Conrad and Husson (2009); Müller
 312 et al. (2008)). Combination of the 2 datasets (coastal uplift and dynamic topography) was
 313 performed in a 0.5 degree-bin because of the high apparent resolution of the dynamic
 314 topography models. Table 3 shows the comparison between the average observed uplift and
 315 the average vertical ground motion possibly due to changes in the dynamic support of the
 316 topography. Figure 8 shows the relationship between the rate of change in the modelled
 317 dynamic topography and measured uplift.

318
 319
 320
 321
 322
 323

Table 3. Comparison of the observed uplift (Pedoja et al. (2011)) with modelled dynamic topography rates of change at the same locations (Conrad and Husson (2009); Müller et al. (2008)). The values are the average of 0.5 degrees bins regarding subduction zones. Note that the uplift observed from Pedoja et al. (2011) consequently differs from the average values of the entire set of observations (0.2227 mm/yr).

	Average uplift rate since the MIS 5e (mm/y)	Average uplift since the MIS 5e (m)
Observed uplift from Pedoja et al. (2011)	0.3533	44.16
Dynamic topography after Conrad and Husson (2009)	0.005	0.625
Dynamic topography after Müller et al. (2008)	-0.029	-3.625

324



325
 326
 327

Figure 8. Uplift rate versus rate of change in dynamic topography for the last Ma.; in red, after Conrad and Husson (2009); in blue, after Müller et al. (2008).

328 According to the tested dynamic topography models, the average contribution to the vertical
 329 motion would be one order of magnitude underneath the observed uplift. In addition to this,
 330 figure 8 and the related correlation coefficient prevent from stating that there is a significant
 331 link between the dynamic topography and the observed coastal uplift rate. Last, the fact that
 332 most coastlines are uplifting suggests that dynamic topography shall not explain this
 333 phenomenon; indeed, uplift and subsidence must overall cancel each other and average to
 334 zero.

335 3.6 Other parameters

336 The other tested parameters do not show any trend with coastal uplift. Their correlation
 337 coefficient is too low to conclude on the robustness of any link between the measured uplift
 338 and tested geodynamic parameters. Among these, we explored the correlation of uplift rates
 339 with the commonly invoked overriding and subducting plate velocities, trench motion,
 340 convergence acceleration, subduction obliquity, oceanic crust age, interplate force and friction

341 force. Figure 9 summarizes the relationship between all the aforementioned parameters and
342 the coastal uplift.

343 **Plate and trench motion**

344 The absolute plate motion comes from Steinberger et al. (2004). In Figure 9 A and B, positive
345 (negative) values of subducting or overriding absolute plate motion indicate a movement
346 toward (away from) the trench. The normal overriding plate velocity does not appear to be
347 correlated with the uplift rate. Although the normal subducting plate velocity visually seems
348 slightly correlated to the uplift rate the correlation coefficient is nearly null (~ 0.02) (Figure
349 9B). Finally, the convergence velocity is also surprisingly not correlated with terrace uplift
350 (Figure 9A), even if we only take into account the trench-normal convergence velocity
351 (Figure 9B). No correlation between trench motion and uplift rate is detectable (Figure 9C).
352 In addition we evaluated the current change in convergence velocity for the plates involved in
353 the Tonga-Kermadec, Japan, South America, Aleutian and Cascadia subduction (Figure 9D)
354 by comparing a compilation of GPS derived, instantaneous velocity data (Sella et al. (2002))
355 to the integrated velocity for the last 3.2 Ma (NUVEL-1A, De Mets et al. (1994)). It is not
356 possible to derive any correlation since the plate velocity change is distributed in patches.
357 Anyway, the visual inspection does not plead for any correlation.

358 **Obliquity**

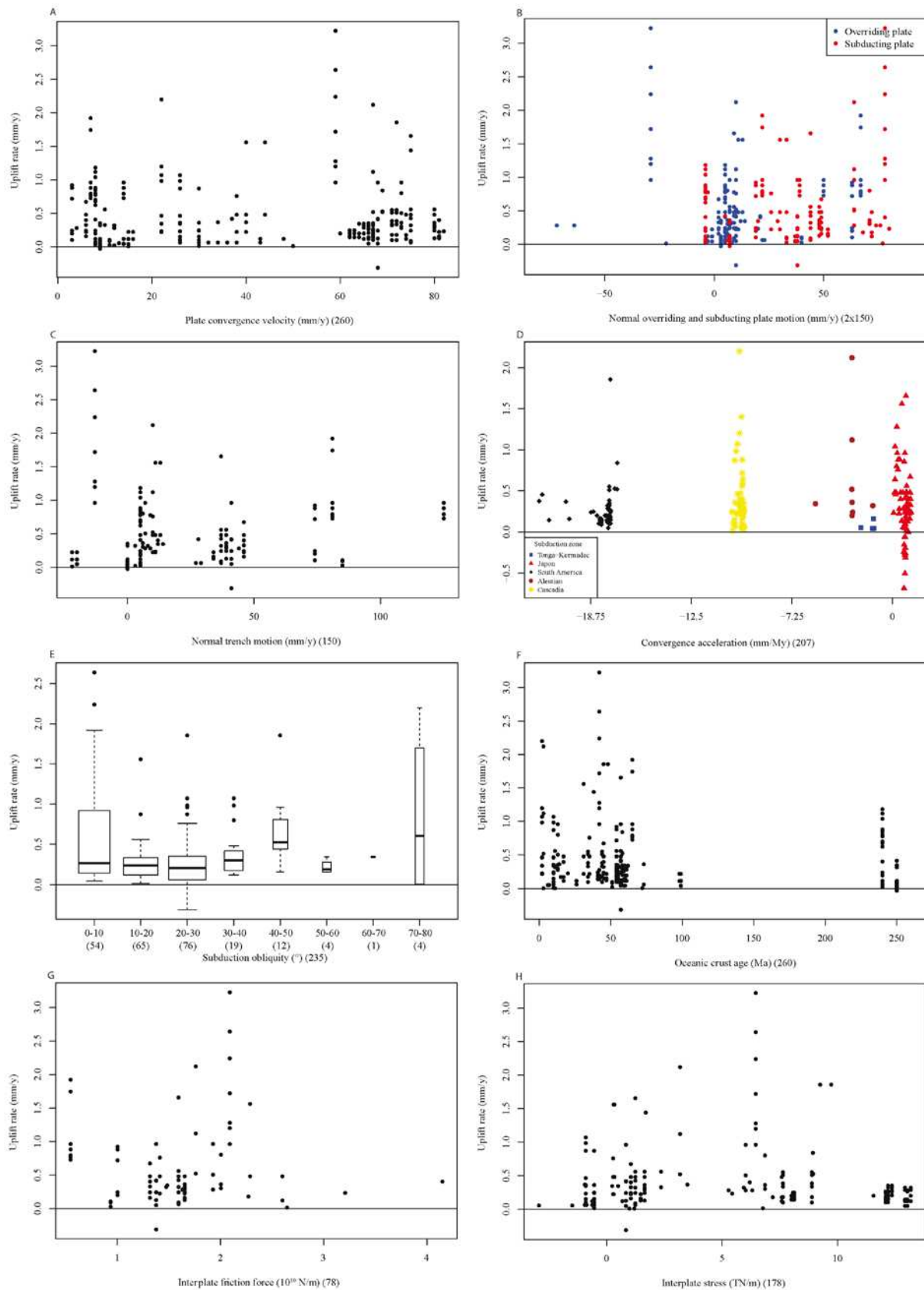
359 The subduction obliquity is calculated using DeMets et al. (1994) NUVEL-1A plate velocity
360 model and Heuret (2005)'s trench azimuth (Figure 9E). An obliquity value of 0° indicates a
361 perfectly orthogonal subduction. The dataset covers a wide range of obliquity values that are
362 well distributed. No trend is observed except a possible slight increase towards normal
363 convergence.

364 **Oceanic crust age**

365 The oceanic crust age is compiled by Heuret and Lallemand (2005) after Müller et al. (1997)
366 and indicates the age of the oceanic crust at the trench. This distribution is not correlated with
367 the uplift rate.

368 **Interplate friction force and interplate force**

369 Figure 9G shows the interplate friction force (*sensu* Lallemand, 1999) vs uplift rate. The
370 interplate force is estimated by Husson (2012) by calculating the mean of the integrated
371 mantle drag from both the overriding and subducting plate (M_d). There is detectable uplift rate
372 correlation neither with the interplate friction force nor with M_d (Figure 9G & H).



373

374 *Figure 9. A: Uplift rate as a function of the convergence rate; B: Uplift rate as a function of the*
 375 *overriding (blue) and subducting plate (red) absolute motion; C: Uplift rate as a function of the*
 376 *absolute trench motion; D: Uplift rate as a function of the convergence variation for the last 3.2*
 377 *Myrs, as the difference between NUVEL-1A and REVEL models, the different subduction zones are*

378 *pictured; E: Uplift rate as a function of the convergence obliquity; F: Uplift rate as a function of*
 379 *the oceanic crust age at the trench; G: Uplift rate as a function of the interplate friction force. H:*
 380 *Uplift rate as a function of the interplate force.*

381 **4. SUMMARY AND DISCUSSION**
 382

383 *Table 4. Linear correlation coefficient between the tested geodynamic parameters and the coastal*
 384 *uplift. Bold lines indicate significant correlation (or anticorrelation) (p-values < 0.01).*

Geodynamic Parameter	Correlation coefficient	Confidence interval (1 σ)	p-values
Subduction obliquity	0.019	[-0.04 0.082]	0.757
Oceanic crust age	-0.148	[-0.208 -0.087]	0.016
Normal Trench motion	0.072	[-0.0101 0.153]	0.382
Interplate force	-0.06	[-0.134 0.015]	0.427
Interplate friction force	0.03	[-0.085 0.144]	0.795
Overriding plate velocity	0.026	[-0.056 0.108]	0.748
Subducting plate velocity	0.239	[0.160 0.315]	0.003
Shallow slab dip	0.286	[0.219 0.350]	4.80x10⁻⁵
Deep slab dip	0.431	[0.368 0.490]	1.70x10⁻⁹
Convergence velocity	0.015	[-0.047 0.077]	0.805
Normal convergence velocity	0.203	[0.124 0.280]	0.012
Convergence acceleration since 3.2 Ma	0.051	[-0.018 0.120]	0.467
Distance to the trench (boxes)	-0.28	[-0.366 -0.189]	0.003
Distance to the trench, in fraction of the distance trench-arc	-0.119	[-0.189 -0.047]	0.031
Distance to the trench (South America transect)	-0.355	[-0.469 -0.229]	0.007
Distance to the trench (Japan-Korea transect)	-0.248	[-0.400 -0.088]	0.128
Distance to the trench (Cascadia transect)	-0.769	[-0.858 -0.637]	3.00x10⁻⁴
Dynamic topography (Conrad and Husson (2009))	0.191	[0.123 0.257]	0.005
Dynamic topography (Müller et al. (2008))	-0.229	[-0.294 -0.162]	9.10x10⁻⁴
Overriding plate tectonic setting	Gently correlated		
Position along the trench	Significantly correlated		
Tectonic regime of the subduction margin	Gently correlated		

385
 386 Table 4 summarises the correlation between observed uplift rates and all tested parameters.
 387 Overall, most of the investigated geodynamic parameters do not seem to influence the uplift
 388 rate. We additionally observed higher uplift rates near lateral slab boundaries. Lallemand et al.
 389 (2005) observe that slab dip is generally higher at slab edge. Slab edges are also known to be
 390 places of high upper mantle toroidal motion, and eventually mantle vertical flow (e.g.,
 391 Funicello et al. (2006); Guillaume et al. (2010); Schellart et al. (2007)). This leads to
 392 important variations in geodynamics at slab edges (Schellart et al. (2011)). Out of all the
 393 tested parameters, two parameters are highly correlated to uplift. First, slab dip shows some
 394 correlation with the uplift rate. Lallemand et al. (2005), in turn, show that the slab dip

395 correlates to the overriding plate tectonic setting. The higher the slab dip is, the more
396 extensive the regime of the overriding plate will be. It is fully coherent with the fact the
397 tectonic setting appears to be linked with uplift rate. But its effect is quite counterintuitive
398 since uplift is possibly related to extension and low uplift to compression.

399 Due to the quasi-absence of subsiding data, it is not possible to tell if accretionary margins are
400 more prone to uplift (and less prone to subsidence) than erosive ones, as shown by the works
401 on subduction tectonic erosion (e.g., Lallemand et al., 1992). However, noticeable is the fact
402 that erosive margins are not devoid of uplift zones despite the fact that intuitively, the forearc
403 material loss associated with tectonic erosion is likely to promote subsidence. The normal
404 faults that have been described in most erosive margins (e.g., Clift and Vannuchi, 2004)
405 should be responsible of the observed uplifts. The difference between erosive/accretionary
406 margins is best expressed in terms of variability of the uplift magnitude, greater for
407 accretionary margins. Large uplifts at erosive margins are possibly inhibited by the forearc
408 material related to the erosive processes.

409 Second and maybe the best correlated parameter to uplift is the distance to the trench which
410 shows in 3 particular transects a rapidly slowing uplift with the distance: we evaluated the
411 characteristic distance of action of the trench to be ~ 300 km, i.e., the trench-arc distance.

412 The main limitation of our approach is the small number of sites evidencing coastal
413 subsidence, partly because measuring subsidence is more difficult than measuring uplift,
414 partly because it is less common. For example, this excludes the Sunda subduction zone due
415 to a lack of observational data. Even if we consider the record is correct for uplifting areas,
416 the input of subsiding areas could enlarge the range of parameters to observe. For example,
417 extrapolating the regression observed for steeply dipping slabs toward gentle dips predict
418 negative values, i.e., subsidence. This will have to be investigated.

419 Another limitation is that “simple” subduction zones associated with a coastline prone to
420 record fossil shores are not so frequent. For example the Tonga-Kermadec and Marianas
421 subduction zones are ocean-ocean subduction zones, with limited subaerial exposure in which
422 vertical displacements can be measured.

423

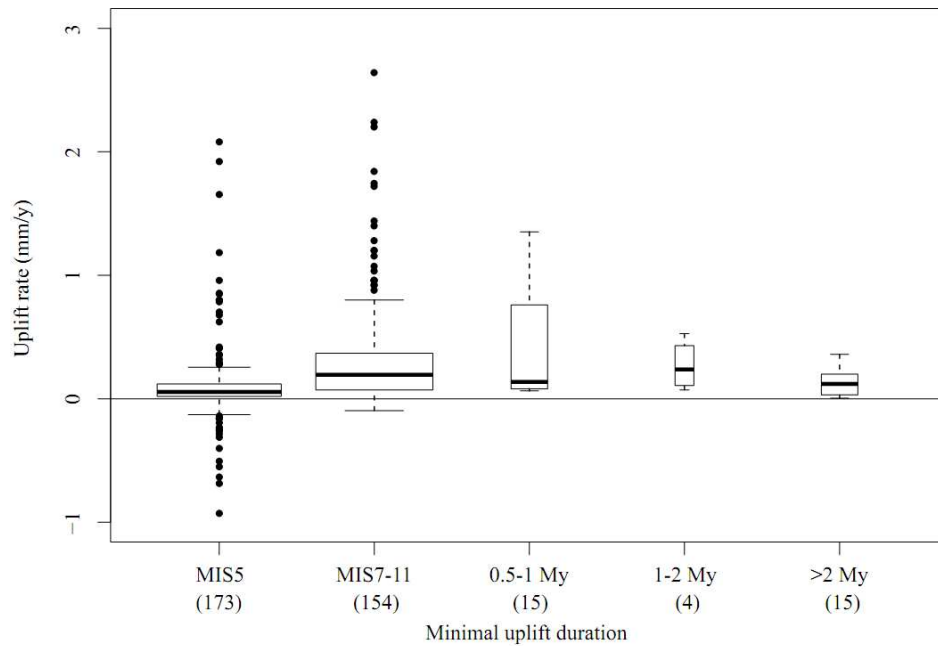
424 A possible reason for the poor correlation between uplift and the geodynamic parameters of
425 subduction zones is that subduction zones correspond to a long-term phenomenon that lasts
426 tens of Myrs. In contrast, the analysis of terraces associated with the MIS5e isotopic stage
427 evidences short term ($\sim 10^5$ years) vertical displacements. Subductions zones evolve slowly
428 through time and their morphology should be in equilibrium with the main geodynamic
429 parameters such as the convergence velocity or the friction at the plate interface. One can
430 expect that short-term coastal uplift (or subsidence) is mostly due to changes in these
431 parameters. We thus explored the variation in subduction velocity and the variation in the
432 dynamic topography but here again we fail at finding any correlation. Finally, the absence of
433 correlation between geodynamics and vertical motion may plead for a local effect (or short in
434 time) causing strong vertical motion. These local effects are preferentially due to roughness of
435 the subducting plate as we illustrate by the examples in the following.

436 (1) In fact, the high uplift rate of E3 (strongly extensive) tectonic setting can come from the
437 position of E3 data close to slab edges (38 data over 40). The north New Hebrides (Vanuatu)
438 subduction zone is typical from E3 tectonic setting. It is marked by back-arc opening but also
439 by many plateau/ridges entering into subduction (Taylor et al. (2005)), probably causing a
440 high variability in uplift rates. They range 0.004-1.896 mm/y, with a median uplift rate of
441 ~ 0.756 mm/y, close to the median value for E3 (Figure 5 and Table 1). This subduction zone
442 clearly questions the origin of the high uplift rate: the extensional setting, the proximity to
443 slab edges, the subduction of asperities like the d'Entrecasteaux ridge (Collot et al. 1985;
444 Taylor et al. 2005), or a slab break-off (Châtelain et al. 1992)? A distribution of decreasing

445 uplift rates westward from the trench to the back arc basins is also clearly documented here
446 (e.g., Collot et al. 1985; Châtelain et al. 1992; Taylor et al., 1987; 2005).

447 (2) The Nazca plate subduction under South America is characterized by a C3 tectonic setting
448 and a moderate uplift rate (median at 0.176 mm/y and range 0.024-0.816 mm/yr; see also the
449 transect Figure 3); none of the points is at (or near) a slab edge. A particular characteristic of
450 this subduction zone is the entrance of some aseismic ridges into the subduction zone
451 (Gutscher et al., 2000), causing the highest uplift values of this area (e.g., Machare and
452 Ortlieb (1992); Martinod et al. (2013); Regard et al. (2010); Saillard et al. (2011)). Of
453 particular interest is the Nazca Ridge entering into the subduction zone in central-south Peru
454 (Machare and Ortlieb (1992); Regard et al. (2010); Saillard et al. (2011)). The contact point of
455 the ridge with the trench is moving southeastward (Hampel (2002), Espurt et al. (2008)).
456 North of this contact point the coastline is subsiding (cf. in Lima, Leroux et al. (2000)), after
457 the Nazca Ridge passed through. Thus the slab buoyancy appears to be a major driving
458 parameter for vertical motion in Peru. Another important fact is that if this subduction zone is
459 characterized by Heuret (2005) as strongly compressive (C3), we note that the forearc
460 behaves differently: the margin is believed to be tectonically erosional (e.g., Lallemand et al.
461 (1992)) and it is sometimes extensional, in particular in the entire northern part of Chile (e.g.,
462 Gonzalez et al., 2003).

463
464 Finally, these examples show that the uplift rate recorded by ancient shorelines mostly
465 concerns the forearc, whose tectonic setting (~100-300 km from the trench) is sometimes
466 disconnected from that of the back-arc area as recorded by Heuret and Lallemand (2005)
467 (~300-500 km). We can hypothesize that the upper plate quickly responds vertically to
468 external factors, as every change in geodynamical setting. Consequently, the subduction zones
469 are generally close to equilibrium with the external forces causing stability (or slowly
470 evolving) in terms of vertical motion. Superimposed on to this geodynamic setting a ridge
471 entrance into subduction is prone to cause significant uplift, maybe more efficiently if the far
472 field upper plate tectonic setting is extensional. That is why high uplift rates are transient and
473 cannot last more than a couple of hundred of thousand years: figure 10 shows that high uplift
474 rates are only found in places uplifting for a short period of time (<1-2 My). The ridge effect
475 is important when the ridge slides along the trench as the Nazca Ridge does (or when a new
476 ridge enters into trench). On the contrary a ridge entering the subduction at the same point for
477 a long time would not cause a temporal change: a good example is the Juan Fernandez Ridge
478 in Chile.



479 *Figure 10. Uplift rate since MIS5 as a function of the observed duration of uplift (maximum age of*
 480 *uplifted shorelines).*
 481

482 5. CONCLUSION

483 We explored the relationship between the observed coastal late Pleistocene uplift rates and
 484 various geodynamic parameters. This statistical study shows that most of the geodynamic
 485 parameters are not related to coastal uplift magnitude. The distance to the trench presents a
 486 slightly correlated signal with the coastal uplift. It is possible this effect ends at ~300 km from
 487 the trench, which approximately corresponds to the position of the volcanic arc. Other slight
 488 correlations have been found between uplift and slab dip, position along the trench and
 489 overriding plate tectonic regime.

490 The main message is that subduction zones are characterized by rapid vertical motion (uplift
 491 but maybe also subsidence as stated in introduction), only part of which being satisfactorily
 492 explained by the geodynamic setting. Over this global setting, strong vertical motion is due to
 493 smaller scale heterogeneities (one can call roughness) of the subducting plate, one typical
 494 example of roughness being a subducting aseismic ridge. Asperity affects more efficiently the
 495 areas close to the trench.

496 ACKNOWLEDGEMENTS

497 This study is based on a dataset produced in the framework of the ANR JCJC GISELE
 498 (Geodynamics of Sea Level, PI. L. Husson) with a support from the INSU/SHOM reliefs de la
 499 Terre program “erosion of rocky coasts” (PI V. Regard). We thank W. P. Schellart (Associated
 500 Editor), M.-A. Gutscher and an anonymous reviewer for their constructive comments.

501 REFERENCES

502
 503 Becker, T.W., 2006. On the effect of temperature and strain-rate dependent viscosity on global
 504 mantle flow, net rotation, and plate-driving forces. *Geophys. J. Int.* 167, 943–957.
 505 doi:10.1111/j.1365-246X.2006.03172.x

506 Becker, T.W., 2008. Azimuthal seismic anisotropy constrains net rotation of the lithosphere.
507 Geophys. Res. Lett. 35, L05303. doi:10.1029/2007GL032928

508 Châtelain, J.-L., Molnar, P., Prévot, R., and Isacks, B.L., 1992. Detachment of part of the
509 downgoing slab and uplift of the New Hebrides (Vanuatu) islands. Geophysical
510 Research Letters 19, 1507–1510.

511 Clift, P., Vannucchi, P., 2004. Controls on tectonic accretion versus erosion in subduction
512 zones: Implications for the origin and recycling of the continental crust. Reviews of
513 Geophysics 42, 2003RG000127.

514 Conrad, C. and Husson, L., 2009. Influence of dynamic topography on sea level and its rate of
515 change. Lithosphere, 1(2): 110-120, doi: 10.1130/L32.1.

516 Collot, J. Y., Daniel J., and Burne R.V., 1985. Recent tectonics associated with the
517 subduction/collision of the d'Entrecasteaux Zone in the central New Hebrides:
518 Structures and processes in subduction zones, Tectonophysics, 112, 325 – 356.

519 DeMets, C., Gordon, R.G., Argus, D.F. and Stein, S., 1994. Effect of recent revisions to the
520 geomagnetic reversal time scale on estimates of current plate motions. Geophysical
521 Research Letters, 21(20): 2191-2194.

522 Espurt, N., Funiciello, F., Martinod, J., Guillaume, B., Regard, V., Faccenna, C. and Brusset,
523 S., 2008. Flat subduction dynamics and deformation of the South American plate:
524 Insights from analog modeling. Tectonics, 27: TC3011, doi:10.1029/2007TC002175.

525 Funiciello, F., Faccenna, C. and Giardini, D., 2004. Role of lateral mantle flow in the
526 evolution of subduction systems: insights from laboratory experiments. Geophysical
527 Journal International, 157: 1393-1406.

528 Funiciello, F., Moroni, M., Piromallo, C., Faccenna, C., Cenedese, A. and Bui, H.A., 2006.
529 Mapping mantle flow during retreating subduction: Laboratory models analyzed by
530 feature tracking. Journal of Geophysical Research - Solid Earth, 111: B03402,
531 doi:10.1029/2005JB003792.

532 Funiciello, F., Faccenna, C., Heuret, A., Lallemand, S., Di Giuseppe, E., Becker, T.W., 2008.
533 Trench migration, net rotation and slab–mantle coupling. Earth and Planetary Science
534 Letters 271: 233–240.

535 Gonzalez, G., Cembrano, J., Carrizo, D., Macci, A. and Schneider, H., 2003. The link between
536 forearc tectonics and Pliocene-Quaternary deformation of the Coastal Cordillera,
537 northern Chile. Journal of South American Earth Sciences, 16: 321-342.

538 Gripp, A.E., Gordon, R.G., 2002. Young tracks of hotspots and current plate velocities.
539 Geophysical Journal International 150, 321–361.

540 Guillaume, B., Moroni, M., Funiciello, F., Martinod, J. and Faccenna, C., 2010. Mantle flow
541 and dynamic topography associated with slab window opening: Insights from
542 laboratory models. Tectonophysics, 496: 83-98.

543 Gutscher, M.A., Malavieille, A., Lallemand, S. and Collot, J.Y., 1999a. Tectonic segmentation
544 of the North Andean margin: impact of the Carnegie Ridge collision. Earth and
545 Planetary Science Letters, 168: 255-270.

546 Gutscher, M.A., Olivet, J.L., Aslanian, D., Eissen, J.P. and Maury, R., 1999b. The “Lost Inca
547 Plateau”: cause of flat subduction beneath Peru? Earth and Planetary Science Letters,
548 171: 335-341.

549 Gutscher, M.A., Spakman, W., Bijwaard, H. and Engdhal, E.R., 2000. Geodynamics of flat
550 subduction: Seismicity and tomographic constraints from the Andean margin.
551 Tectonics, 19(5): 814-833.

552 Hampel, A., 2002. The migration history of the Nazca Ridge along the Peruvian active
553 margin: a re-evaluation. Earth and Planetary Science Letters, 203(665-679).

554 Heuret, A., 2005. Dynamique des zones de subduction: étude statistique globale et approche
555 analogique, PhD, University of Montpellier, 241 p.

556 Heuret, A., Lallemand, S., 2005. Plate motions, slab dynamics and back-arc deformation.
557 Physics of the Earth and Planetary Interiors 149: 31–51.

558 Husson, L., 2012. Trench migration and upper plate strain over a convecting mantle. Physics
559 of the Earth and Planetary Interiors, 212-213: 32-43.

560 Kopp, R.E., Simons, F.J., Mitrovica, J.X., Maloof, A.C. and Oppenheimer, M., 2009.
561 Probabilistic assessment of sea level during the last interglacial stage. Nature, 462:
562 863-867.

563 Kreemer, C., 2009. Absolute plate motions constrained by shear wave splitting orientations
564 with implications for hot spot motions and mantle flow. J. Geophys. Res.-Solid Earth
565 114, B10405. doi:10.1029/2009JB006416

566 Lajoie, K.R., Ponti, D.J., II, C.L.P., Mathieson, S.A. and Sarna-Wojcicki, A.M., 1991.
567 Emergent marine strandlines and associated sediments, coastal California; a record of
568 Quaternary sea-level fluctuations, vertical tectonic movements, climatic changes, and
569 coastal processes, in: Quaternary Nonglacial Geology: Conterminous U.S. Geological
570 Society of America, Boulder, Colorado: 190-203.

571 Lallemand, S., 1999. La subduction océanique. Gordon and Breach Science Publishers.

572 Lallemand, S., Heuret, A. and Boutelier, D., 2005. On the relationships between slab dip,
573 back-arc stress, upper plate absolute motion, and crustal nature in subduction zones.
574 Geochemistry, Geophysics, Geosystems, 6: Q09006, doi:10.1029/2005GC000917.

575 Lallemand, S., Schnurle, P. and Manoussis, S., 1992. Reconstruction of Subduction Zone
576 Paleogeometries and Quantification of Upper Plate Material Losses Caused by
577 Tectonic Erosion. Journal of Geophysical Research, 97: 217-239.

578 Leroux, J.P., Correa, C.T. and Alayza, F., 2000. Sedimentology of the Rimac-Chillon alluvial
579 fan at Lime, Peru, as related to Plio-Pleistocene sea-level changes, glacial cycles and
580 tectonics. Journal Of South American Earth Sciences, 13: 499-510.

581 Lowry, A.R., Ribe, N.M. and Smith, R.B., 2000. Dynamic elevation of the Cordillera, western
582 United States. Journal of Geophysical Research: Solid Earth, 105: 23371-23390.

583 Machare, J. and Ortlieb, L., 1992. Plio-Quaternary vertical motions and the subduction of the
584 Nazca Ridge, central coast of Peru. Tectonophysics, 205: 97-108.

585 Martinod, J., Guillaume, B., Espurt, N., Faccenna, C., Funicello, F. and Regard, V., 2013.
586 Effect of aseismic ridge subduction on slab geometry and overriding plate
587 deformation: Insights from analogue modeling. Tectonophysics, 588: 39-55.

588 Müller, R., Roest, W., Royer, J.Y., Gahagan, L. and Sclater, J., 1997. Digital isochrons of the
589 world's ocean floor. Journal of Geophysical Research, 104: 3211-3214.

590 Müller, R.D., Sdrolias, M., Gaina, C., Steinberger, B. and Heine, C., 2008. Long-term sea
591 level fluctuations driven by ocean basin volume change. Science, 319: 1357-1362.

592 O'Leary, M.J., Hearty, P.J., Thompson, W.G., Raymo, M.E., Mitrovica, J.X. and Webster,
593 J.M., 2013. Ice sheet collapse following a prolonged period of stable sea level during
594 the last interglacial. Nature Geoscience, 6: 796-800.

595 O'Neill, C., Müller, D., Steinberger, B., 2005. On the uncertainties in hot spot reconstructions
596 and the significance of moving hot spot reference frames. Geochem. Geophys.
597 Geosyst. 6, Q04003. doi:10.1029/2004GC000784

598 Pearson, K., 1896. Mathematical Contributions to the Theory of Evolution. III. Regression,
599 Heredity and Panmixia. Philosophical Transactions of the Royal Society of London
600 187: 253-318.

601 Pedoja, K., Husson, L., Johnson, M.E., Melnick, D., Witt, C., Pochat, S., Mexer, M.,
602 Delcaillau, B., Pinegina, T., Poprawski, Y., Authemayou, C., Elliot, M., Regard, V. and
603 Garestier, F., in press. Staircase construction of Quaternary and Upper Cenozoic
604 sequences of strandlines caused by sea level oscillations and tectonic uplift. Earth-
605 Science Reviews, in press.

606 Pedoja, K., Husson, L., Regard, V., Cobbold, P.R., Ostanciaux, E., Johnson, M.E., Kershaw,
607 S., Saillard, M., Martinod, J., Gurgerot, L., Weill, P. and Delcaillau, B., 2011. Relative
608 sea-level fall since the last interglacial stage: Are coast uplifting worldwide? *Earth-*
609 *Science Review*, 108: 1-15.

610 Pirazzoli, P.A., Radtke, U., Hantoro, W.S., Jouannic, C., Hoang, C.T., Causse, C. and Besth,
611 M.B., 1993. A one million-year-long sequence of marine terraces on Sumba Island,
612 Indonesia. *Marine Geology*, 109: 221-236.

613 RDevelopment Core Team, 2010. R: A language and environment for statistical computing. R
614 Foundation for Statistical Computing <http://www.R-project.org/>.

615 Regard, V., Saillard, M., Martinod, J., Audin, L., Carretier, S., Pedoja, K., Riquelme, R.,
616 Paredes, P. and Hérail, G., 2010. Renewed uplift of the Central Andes Forearc revealed
617 by coastal evolution during the Quaternary. *Earth and Planetary Science Letters*, 297:
618 199-210.

619 Saillard, M., Hall, S.R., Audin, L., Farber, D.L., Regard, V. and Hérail, G., 2011. Andean
620 coastal uplift and active tectonics in southern Peru: ^{10}Be surface exposure dating of
621 differentially uplifted marine terrace sequences (San Juan de Marcona, $\sim 15.4^\circ\text{S}$).
622 *Geomorphology*, 128: 178-190.

623 Schellart, W.P., 2011. A subduction zone reference frame based on slab geometry and
624 subduction partitioning of plate motion and trench migration. *Geophys. Res. Lett.* 38,
625 L16317. doi:10.1029/2011GL048197

626 Schellart, W.P., Freeman, J., Stegman, D.R., Moresi, L. and May, D., 2007. Evolution and
627 diversity of subduction zones controlled by slab width. *Nature*, 446: 308-311.

628 Schellart, W.P., Stegman, D.R., Farrington, R.J. and Moresi, L., 2011. Influence of lateral slab
629 edge distance on plate velocity, trench velocity, and subduction partitioning. *Journal of*
630 *Geophysical Research - Solid Earth*, 116: B10408, doi:10.1029/2011JB008535.

631 Schellart, W.P., Stegman, D.R., Freeman, J., 2008. Global trench migration velocities and slab
632 migration induced upper mantle volume fluxes: Constraints to find an Earth reference
633 frame based on minimizing viscous dissipation. *Earth-Sci. Rev.* 88, 118–144.
634 doi:10.1016/j.earscirev.2008.01.005

635 Sella, G.F., Dixon, T.H. and Mao, A.L., 2002. REVEL: A model for recent plate velocities
636 from space geodesy. *Journal of Geophysical Research - Solid Earth*, 107(B4): ETG-11,
637 doi:10.1029/2000JB000033.

638 Stafford, K., Mylroie, J., Taborosi, D., Jenson, J. and Mylroie, J., 2005. Karst development on
639 Tinian, commonwealth of the Northern Mariana Islands: Controls on dissolution in
640 relation to the Carbonate Island Karst Model. *Journal of Cave and Karst studies*, 67:
641 14-27.

642 Steinberger, B., Sutherland, R. and O'Connell, R.J., 2004. Prediction of Emperor-Hawaii
643 seamount locations from a revised model of global plate motion and mantle flow.
644 *Nature*, 430: 167-173.

645 Tassara, A., 2005. Interaction between the Nazca and South American plates and formation of
646 the Altiplano–Puna plateau: Review of a flexural analysis along the Andean margin
647 (15° – 34°S). *Tectonophysics*, 399: 39-57.

648 Tassara, A., Hackney, C. and Kirby, R., 2007. Elastic thickness structure of South America
649 estimated using wavelets and satellite-derived gravity data. *Earth and Planetary*
650 *Science Letters*, 253: 17-36.

651 Taylor, F.W., Frohlich, C., Lecolle, J., Strecker, M., 1987. Analysis of partially emerged
652 corals and reef terraces in the central Vanuatu Arc: Comparison of contemporary
653 coseismic and nonseismic with quaternary vertical movements. *Journal of*
654 *Geophysical Research: Solid Earth* 92, 4905–4933.

655 Taylor, F.W., Mann, P., Bevis, M.G., Edwards, R.L., Cheng, H., Cutler, K.B., Gray, S.C., Burr,
656 G.S., Beck, J.W., Phillips, D.A., Cabioch, G. and Recy, J., 2005. Rapid forearc uplift
657 and subsidence caused by impinging bathymetric features: Examples from the New
658 Hebrides and Solomon arcs. *Tectonics*, 24: TC6005, doi:10.1029/2004TC001650.

659 Tukey, J.W., 1977. *Exploratory data analysis*, Addison-Wesley Series in Behavioral Science:
660 Quantitative Methods, Reading, Mass., vol. 1 Addison-Wesley.

661 Waelbroeck, C., Labeyrie, L., Michel, E., Duplessy, J.C., McManus, J.F., Lambeck, K. and
662 Labracherie, M., 2002. Sea level and deep water temperature changes derived from
663 benthics foraminifera isotopic records. *Quaternary science reviews*, 21(1-3): 295-305.

664 Yañez, G.A., Ranero, C.R., Huene, R.v. and Diaz, J., 2001. Magnetic anomaly interpretation
665 across the southern central Andes (32 degrees-34 degrees S): The role of the Juan
666 Fernandez Ridge in the late Tertiary evolution of the margin. *Journal of Geophysical*
667 *Research-Solid Earth*, 106: 6325-6345.

668
669